



**HAL**  
open science

# High-temperature Ionization-induced Synthesis of Biologically Relevant Molecules in the Protosolar Nebula

David V Bekaert, Sylvie Derenne, Laurent Tissandier, Yves Marrocchi,  
Sébastien Charnoz, Christelle Anquetil, Bernard Marty

► **To cite this version:**

David V Bekaert, Sylvie Derenne, Laurent Tissandier, Yves Marrocchi, Sébastien Charnoz, et al.. High-temperature Ionization-induced Synthesis of Biologically Relevant Molecules in the Protosolar Nebula. *The Astrophysical Journal*, 2018, 859 (2), pp.142. 10.3847/1538-4357/aabe7a . hal-02357535

**HAL Id: hal-02357535**

**<https://hal.univ-lorraine.fr/hal-02357535>**

Submitted on 10 Nov 2019

**HAL** is a multi-disciplinary open access archive for the deposit and dissemination of scientific research documents, whether they are published or not. The documents may come from teaching and research institutions in France or abroad, or from public or private research centers.

L'archive ouverte pluridisciplinaire **HAL**, est destinée au dépôt et à la diffusion de documents scientifiques de niveau recherche, publiés ou non, émanant des établissements d'enseignement et de recherche français ou étrangers, des laboratoires publics ou privés.



# High-temperature Ionization-induced Synthesis of Biologically Relevant Molecules in the Protosolar Nebula

David V. Bekaert<sup>1</sup> , Sylvie Derenne<sup>2</sup>, Laurent Tissandier<sup>1</sup>, Yves Marrocchi<sup>1</sup> , Sebastien Charnoz<sup>3</sup> ,  
Christelle Anquetil<sup>2</sup>, and Bernard Marty<sup>1</sup>

<sup>1</sup> Centre de Recherches Pétrographiques et Géochimiques, UMR 7358 CNRS—Université de Lorraine, 15 rue Notre Dame des Pauvres, BP 20, F-54501 Vandoeuvre-lès-Nancy, France; [dbekaert@crpg.cnrs-nancy.fr](mailto:dbekaert@crpg.cnrs-nancy.fr)

<sup>2</sup> METIS, UMR CNRS 7619, EPHE-Sorbonne Université, 4 Place Jussieu, F-75252 Paris Cedex 05, France

<sup>3</sup> Institut de Physique du Globe/Université Paris Diderot/CEA/CNRS, F-75005 Paris, France

Received 2018 January 29; revised 2018 March 30; accepted 2018 April 13; published 2018 June 1

## Abstract

Biologically relevant molecules (hereafter biomolecules) have been commonly observed in extraterrestrial samples, but the mechanisms accounting for their synthesis in space are not well understood. While electron-driven production of organic solids from gas mixtures reminiscent of the photosphere of the protosolar nebula (PSN; i.e., dominated by CO–N<sub>2</sub>–H<sub>2</sub>) successfully reproduced key specific features of the chondritic insoluble organic matter (e.g., elementary and isotopic signatures of chondritic noble gases), the molecular diversity of organic materials has never been investigated. Here, we report that a large range of biomolecules detected in meteorites and comets can be synthesized under conditions typical of the irradiated gas phase of the PSN at temperatures = 800 K. Our results suggest that organic materials—including biomolecules—produced within the photosphere would have been widely dispersed in the protoplanetary disk through turbulent diffusion, providing a mechanism for the distribution of organic meteoritic precursors prior to any thermal/photoprocessing and subsequent modification by secondary parent body processes. Using a numerical model of dust transport in a turbulent disk, we propose that organic materials produced in the photosphere of the disk would likely be associated with small dust particles, which are coupled to the motion of gas within the disk and therefore preferentially lofted into the upper layers of the disk where organosynthesis occurs.

*Key words:* meteorites, meteors, meteoroids – minor planets, asteroids: general – protoplanetary disks

## 1. Introduction

Comets and asteroids (and by extension meteorites) are the leftover solids of the formation and evolution of the solar system. Both are composed of an important proportion of organic materials ranging from simple molecules to macromolecular assemblies. For instance, comets contain a large proportion of complex organic materials (Capaccioni et al. 2015), with (i) glycine, the simplest proteinaceous amino acid, having been detected in both the cometary samples returned from the stardust mission (Elsila et al. 2009) and the coma of comet 67P/Churyumov–Gerasimenko (Altwegg et al. 2016), and (ii) high-molecular-weight organic matter (Fomenkova et al. 1994). Likewise, an extreme molecular complexity has been reported in carbonaceous chondrites (Schmitt-Kopplin et al. 2010), including a large range of biologically relevant molecules (Botta & Bada 2002). The origin of biomolecules in extraterrestrial bodies is not yet understood while it is of prime interest since external deliveries to the early Earth may have constituted an essential source of prebiotic molecules that contributed to the emergence of life (Chyba & Sagan 1992). Such exogenous supplies of organic materials could have occurred during episodes of large bombardment (e.g., during either a late veneer episode or the Terrestrial Late Heavy Bombardment around 4.0–3.8 Gyr ago) or through the continuous infall of interplanetary dust particles (IDPs; Whittet 1997).

From the interstellar medium (ISM) to the Earth's surface, the processes by which organic molecules were formed and made successively more complex vary over environmental conditions, depending on the availability of carbon and energy. Laboratory studies aiming at reproducing natural pathways of OM synthesis have proposed a series of mechanisms accounting for the presence of OM in many reservoirs of the solar system. Laboratory experiments simulating the photochemical and thermal processing of interstellar icy grains predict a wide variety of interstellar biomolecules including amino acids and nucleobases, which have never been unambiguously detected in the ISM (Nuevo 2011)—the detection of interstellar glycine being still under debate (Snyder et al. 2005). Biomolecules synthesized in the laboratory under conditions relevant to the ISM include aldehydes, simple sugars (some of which have been detected in the ISM; Hollis et al. 2000), urea, glycerol (and a number of its derivatives), hydantoin, uracil, and amino acids, especially glycine, as well as amphiphilic molecules (see Nuevo 2011 for a review). If present in the ISM, these molecules could have been delivered to the protoplanetary disk (PPD) and incorporated into the meteorite parent bodies, or (partly) destroyed en route into the disk via thermal and stellar UV processing.

As an alternative, the molecular diversity observed in meteorites could have been established during aqueous alteration processes on their parent body (e.g., aqueous alteration of polycyclic aromatic hydrocarbons, Shock & Schulte 1990; or interstellar hexamethylenetetramine, Vinogradoff et al. 2017), where warm and slightly alkaline conditions could have been favorable for the formose reaction to occur (Kopetzki & Antonietti 2011). Recently, a one-pot hydrothermal synthesis



Original content from this work may be used under the terms of the [Creative Commons Attribution 3.0 licence](https://creativecommons.org/licenses/by/3.0/). Any further distribution of this work must maintain attribution to the author(s) and the title of the work, journal citation and DOI.

of amino acid precursors along with macromolecular chondritic insoluble organic matter (IOM) has been proposed to occur during planetesimal aqueous activity (Kebukawa et al. 2017).

A third possibility to account for the wide diversity of biomolecules within meteorites is formation by organosynthesis within the protosolar nebula (PSN). The Fischer–Tropsch-type (FTT) catalytic reduction of CO by hydrogen in the presence of  $\text{NH}_3$  is a possible source of organic materials and amino acids (Hayatsu et al. 1971; Nuth et al. 2008). The action of electric discharge on a mixture of  $\text{CH}_4$ ,  $\text{N}_2$ , and  $\text{H}_2\text{O}$  with traces of  $\text{NH}_3$  also produces nonprotein amino acids including those found in the Murchison meteorite (Wolman et al. 1972). Interestingly, weakly to fully ionized regions (i.e., plasma environments) are common in PPDs (Fromang et al. 2002; Walsh et al. 2012) and laboratory simulations of organosynthesis from an ionized gas-phase reminiscent of radical-rich plasma environments in the PSN (the Nebulotron experiments) have succeeded in reproducing key specific features of the chondritic IOM, including the soluble/insoluble proportions and the hydrocarbon backbone molecular structure (Biron et al. 2015), the elementary and isotopic patterns observed for chondritic noble gases (Kuga et al. 2015), as well as the occurrence of D/H hot and cold spots (Robert et al. 2017).

Here, we investigate the possible occurrence of biomolecules in organic materials synthesized from an ionized gas phase reminiscent of the PSN photosphere, where nitrogen and oxygen are initially supplied as  $\text{N}_2$  (20%) and CO (60%), in addition to  $\text{H}_2$  (20%). The PSN photosphere corresponds here to the irradiated upper layers of the disk, exposed to stellar UV photons and X-rays and interstellar UV photons and cosmic rays. Under the canonical PSN composition, CO and  $\text{N}_2$  molecules represent the main carrier of carbon and nitrogen atoms ( $\text{CO}/\text{CH}_4 = 5\text{--}20$ ),  $\text{N}_2/\text{NH}_3 = 10\text{--}100$  even if  $\text{H}_2$  is largely dominant ( $\text{CO}/\text{H}_2 \sim 6.10^{-4}$ ,  $\text{N}_2/\text{H}_2 \sim 1.10^{-4}$ ; Iro et al. 2003). The photodissociation of CO molecules was likely effective throughout the PSN (Visser et al. 2009). The highest degrees of ionization, fractional abundances of electrons, and organic radical densities are reached in the upper layers of the disk, directly exposed to strong UV fields from the early Sun and from the ISM (Walsh et al. 2012), where most of the PSN organosynthesis is thus expected to occur (see Kuga et al. 2015 for further details). Interestingly, the remarkable variations observed for the stable isotopes of hydrogen, nitrogen, and oxygen among solar system objects and reservoirs may be accounted for by isotope fractionation during photodissociation by far-UV (FUV) light and subsequent photochemistry of diatomic molecules (e.g., CO,  $\text{N}_2$ ,  $\text{H}_2$ ; Chakraborty et al. 2008, 2014; Muskatel et al. 2011).

Through the use of a high-vacuum Nebulotron experiment we show that organic material can be synthesized within the irradiated upper layers of the PSN. Analysis of the molecular composition of the soluble organic matter (SOM; Neb-SOM) and IOM (Neb-IOM) fractions was carried out by gas chromatography–mass spectrometry (GC–MS) after trimethylsilyl derivatization and by Curie point pyrolysis GC–MS in the presence of tetramethylammonium hydroxide (TMAH)—these derivatizations allow the detection of polar molecules. We discuss the biological interest of several molecules detected in the SOM and IOM recovered from the Nebulotron experiment and address the astrophysical relevance and implications of organosynthesis in the hot and irradiated photosphere of the

PSN, before subsequent distribution throughout the PPD. The spreading of organic materials synthesized in the photosphere of the disk is tested using a simple approach based on a numerical model of dust transport in a turbulent PPD (Charnoz et al. 2011; Charnoz & Taillifet 2012). This approach involves several uncertainties, about which we are explicit, but allows the general outlines of organic materials transport from the photosphere of the PSN to be evaluated.

## 2. Materials and Method

### 2.1. The Nebulotron Synthesis

The Nebulotron consists of a high-vacuum glass line in which adjustable gas mixtures can be flowed through a microwave (2.45 GHz) plasma discharge. For the purpose of this study, an all-metal set was used to build a high-vacuum reactor where the reaction chamber only is made from Pyrex glass, thus precluding the use of any organic joint. Before experiments, the whole system was pumped by a turbomolecular pump and baked for at least two days at  $\sim 180^\circ\text{C}$ . Typical pressure before starting an experiment was  $\sim 1.10^{-6}$  mbar at room temperature. A high purity gas-mixture of CO (60%),  $\text{N}_2$  (20%), and  $\text{H}_2$  (20%) was then flowed continuously through the plasma discharge using high-vacuum digital mass flow controllers. The total pressure in the reactor was  $\sim 1$  mbar, as is commonly used for plasma experiments (see, e.g., Biron et al. 2015; Kuga et al. 2015, 2017; Robert et al. 2017) because at lower pressure the mean free path of electrons becomes too high relative to the size of our reactor. In such a case, almost no collision would occur between electrons and diatomic molecules with all electrons being neutralized onto the walls of the quartz tube. The power input of the microwave discharge was set to 50 W and the plasma was activated for 16 hr. Under these conditions, electrons and heavy particles at 800–1000 K induce the dissociation and ionization of molecular and atomic species (Kuga et al. 2015), leading to the condensation of ions and/or radicals and to the growth of solid particles onto the quartz tube surface. At the end of the experiment, solids were recovered by gently scratching the surface of the quartz reactor. Averaged solid production rates, computed as the total mass of organic materials recovered at the end of the experiment divided by the duration of the synthesis, are only indicative as they do not take into account the fractions of organic materials that are either carried away by the gas, destroyed in the reaction chamber, or lost during final collection. The organic condensates were then stored inside a desiccator at room temperature until they were recovered for separation by organic solvent extraction.

### 2.2. Scanning Electron Microscopy

Secondary electron imaging of organic materials produced in the high-vacuum Nebulotron and deposited in situ on a silicon wafer placed at the bottom of the quartz tube reactor was made at Centre de Recherches Pétrographiques et Géo-chimiques (CRPG), Nancy, France, using a scanning electron microscope (SEM) JEOL JSM-6510 equipped with an Energy Dispersive X-ray Genesis detector. A 3 nA electron beam accelerated at 15 kV was used for the observations.

### 2.3. Soluble Organic Matter (SOM)–Insoluble Organic Matter (IOM) Separation

The soluble fraction of the plasma-produced organic materials was extracted by stirring at room temperature in a 2:1 v/v mixture of dichloromethane and methanol. The extract was separated from the insoluble residue through centrifugation at 3500 rotations per minute and 4°C for 30 minutes. The supernatant was further concentrated using rotary evaporation and conserved in pyridine, a polar aprotic solvent for GC–MS analysis. The insoluble pellet (IOM) was dried under nitrogen. The mass balance was achieved by weighting the IOM and SOM after their separation and by comparing their sum to the initial mass of organic materials recovered from the Nebulotron synthesis.

### 2.4. Gas Chromatography–Mass Spectrometry (GC–MS) and Curie Point Pyrolysis GC–MS (Py GC–MS)

Analysis of the SOM and IOM of the Nebulotron were carried out by GC–MS of trimethylsilyl (TMS) derivatives and by Py GC–MS in the presence of tetramethylammonium hydroxide (TMAH), respectively (Remusat et al. 2005; Gallois et al. 2007). For the TMS derivatization, 50  $\mu$ L of pyridine solution of the Neb-SOM are dried at 40°C under a N<sub>2</sub> flux and further added to 50  $\mu$ L of BSTFA/TMCS: 99/1. After heating at 70°C for 30 minutes and drying at 40°C under a N<sub>2</sub> flux, the residue was dissolved in 50  $\mu$ L of pyridine. 1  $\mu$ L of the resulting solution was injected in GC–MS. The GC–MS device was an Agilent Technologies 6890N gas chromatograph coupled with an Agilent Technologies 5973 Network mass spectrometer. A fused silica capillary column coated with chemically bound Restek RXi-5SilMS (30 m  $\times$  0.25 mm i.d., 0.5  $\mu$ m film) was used in a GC oven programmed from 80°C (30 s) to 100°C at 10°C minutes<sup>-1</sup> and from 100°C to 320°C at 4°C minutes<sup>-1</sup> with He as carrier gas at 1 mL mn<sup>-1</sup>. The injector temperature was 280°C in split mode. The mass spectrometer was operated with an electron energy of 70 eV, an ion source temperature of 220°C, and by scanning masses from 29 to 700 amu at 2.2 scan s<sup>-1</sup>.

Pyrolysis was performed using tubular ferromagnetic wires with a Curie temperature of 650°C. The wires were inductively heated using a high-frequency generator (Pilodist Curie point pyrolyzer) up to Curie temperature and maintained at this temperature for 9.9 s. For the TMAH derivatization, a few milligrams of IOM were placed in the pyrolysis wire prior to addition of a few microliters of TMAH at 25% in methanol. The pyrolysis unit was coupled to a Trace GC Ultra-DSQ MS device (ThermoFischer Technologies). The GC oven program included a first isothermal step at 50°C for 10 minutes prior to heating to 320°C at 2°C minutes<sup>-1</sup> and the MS scan ranged from 29 to 800 amu at 2 scan s<sup>-1</sup>.

Identification of the different compounds in both SOM and IOM pyrolysate was based on mass spectra, GC retention times, and comparison with literature data.

### 2.5. Numerical Simulations

Numerical simulations were carried out using the Lagrangian Implicit Dust Transport in 3D (LIDT3D) code developed by Charnoz et al. (2011, 2015), Charnoz & Taillifet (2012), Taillifet et al. (2014), and Charnoz et al. (2015). This numerical model simulates the diffusive transport of dust particles in a turbulent PPD using Lagrangian numerical simulations in combination

with the Eulerian turbulent diffusion formalism, where representative particles (called “super-particles”) are followed individually in the disk, taking into account gas drag and turbulent diffusion modeled as a stochastic process (Charnoz et al. 2011, 2015; Charnoz & Taillifet 2012; Taillifet et al. 2014). Here, we implemented the synthesis of organic materials from the photosphere of the PPD. Importantly, we stress that defining absolute production rates for organic materials synthesized in the photosphere of the PSN is extremely challenging since the effect(s) of different variables (e.g., degree of ionization of the gas, local pressure, gas composition) on the production rate are not yet constrained. In particular, H<sub>2</sub> is largely dominant in a PSN, while CO dominates the composition of the gas phase in the Nebulotron experiment. In the present study, we thus propose an a priori approach based on arbitrary production rates allowing the general sketch of the transport of organic materials synthesized in the photosphere of the disk to be evaluated. These production rates, which are orders of magnitude lower than the actual production rates derived from the Nebulotron experiments, are given in the respective figure captions. In this simple approach, we also consider that all grains have an initial budget of organic matter that is proportional to the volume of the particle. This component is a proxy of the potential inheritance from alternative processes of organosynthesis (e.g., from the ISM, by FTT reaction and/or aqueous alteration processes).

We computed the 3D transport of 30,000 super-particles subject to gravitational settling, radial drift, and turbulent diffusion, starting from a homogeneous disk (Charnoz et al. 2011). Thermal structure was set as  $T(r) = 500 \left(\frac{r}{1 \text{ au}}\right)^{-1/2}$  K, where  $r$  is the distance from the central star. Particle granulometric cumulative distribution was computed as  $x^{-2.5}$  between 1  $\mu$ m and 1 cm in radius, in agreement with telescopic observations (Sicilia-Aguilar et al. 2011). The turbulence parameter  $\alpha$  was set to 10<sup>-2</sup> in order to adequately model the highly turbulent motion of particles in the upper layers of the disk, where organosynthesis occurs. We considered the presence of a dead zone from 1 to 6 au, in which the turbulence parameter  $\alpha$  was set to 10<sup>-4</sup>. In this laminar and non-accreting region of the disk, the first planetesimals are expected to form because of low fragmentation rates and low radial drift (Birnstiel et al. 2010; Charnoz & Taillifet 2012).

For each dust particle of the simulation, we considered an organic matter (SOM + IOM) content that increases when the particle is located in the photosphere of the disk. Because of their sticking efficiency (Kouchi et al. 2002), we assume that organic materials synthesized in the photosphere likely stick to the dust particles present in the local environment. The final amount of organic materials thus trapped onto the surface of a grain will depend on: (i) the surface of the grain, and (ii) the time the particle spent within the photosphere of the disk. The photosphere of the disk is taken as  $2 \times H$  (that is mostly relevant in the irradiation-dominated regions of the disk, beyond 10 au—see, e.g., Figure 9 of Baillie & Charnoz 2014), where  $H$  is the local pressure height scale (see, e.g., Fromang & Papaloizou 2006). At time zero ( $t_0$ ), all particles are randomly distributed throughout the system (from 0.3 to 50 au). After 500 years, when good mixing conditions have been reached, the OM synthesis starts in the photosphere and its subsequent transport within the disk is computed. Note that grain size evolution through fragmentation or coagulation (Ciesla 2006) was not considered in this study, as it would have drastically

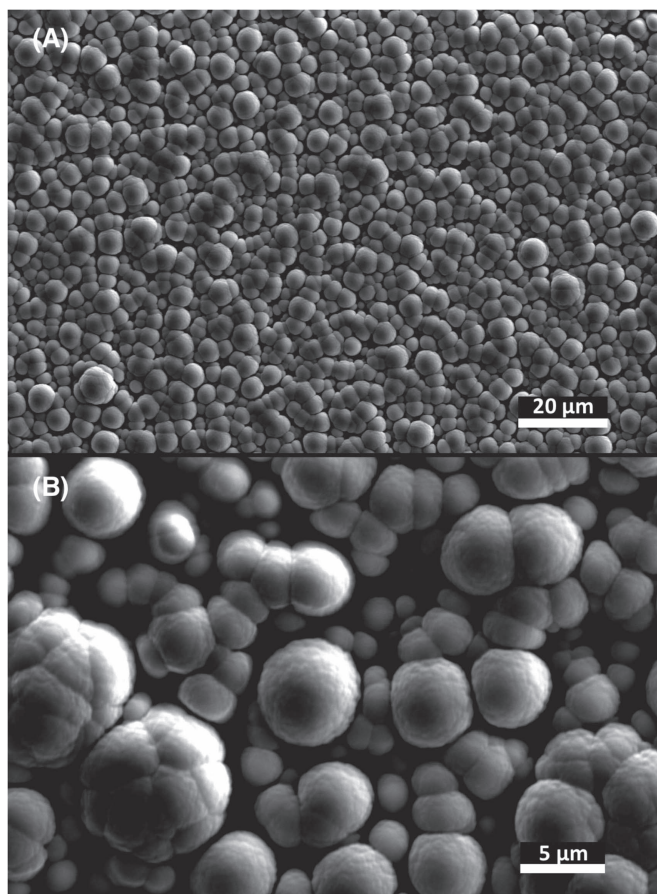


**Figure 1.** Secondary electron imaging (15 kV) of organic materials produced in the high-vacuum Nebulotron and deposited in situ on a silicon wafer placed at the bottom of the quartz tube reactor (magnification A:  $\times 900$ , B:  $\times 3300$ ). We observe free  $\mu\text{m}$ -sized globules as well as larger globule aggregates of several microns in radius.

complicated the tracking of organic materials from one particle to another one. This limitation is discussed in Section 5.2.

### 3. Scanning Electron Imaging of the Nebulotron Condensates

Analogs of organic globules, which have been found in carbonaceous chondrite meteorites and IDPs (De Gregorio et al. 2010), are observed when a silicon wafer is set in the reaction chamber of the Nebulotron for in situ deposition of organic materials (see the Scanning Electron Microscopy image: Figure 1). Similar structures have already been observed from plasma experiments using benzene and anthracene (Saito & Kimura 2009). We observe that single globules of the Neb-OM have diameters of about  $1\ \mu\text{m}$ , although most globules are aggregated to form several  $\mu\text{m}$ -sized spherical structures (Figure 1).

### 4. Chemical Diversity and Biological Interest of the Nebulotron SOM and IOM

After 16 hr of organosynthesis, 54 mg of organic materials were produced in the plasma discharge, thus corresponding to a minimum production rate of  $\sim 0.3\ \text{mg}\ \text{hr}^{-1}$ , of which 80% are IOM and 20% SOM. The GC-MS trace of the SOM and the Py GC-MS trace of the IOM are given in Figure 2. The list of

molecules identified in GC/MS and Py GC/MS are given in Tables 1 and 2, respectively.

While only SOMs are formed through laboratory simulations of the photochemical and thermal processing of interstellar ices (De Marcellus et al. 2016), Nebulotron experiments classically produce both soluble and insoluble materials (Biron et al. 2015). The SOM/IOM ratio of the Nebulotron condensate is 0.25, in agreement with the ratios reported for meteoritic OM, from 0.01 in the Tagish Lake chondrite to 0.3 in the Murchison and Murray CM chondrites (Pizzarello et al. 2006). A large molecular diversity is observed for the SOM and IOM of the Nebulotron condensates, with oxygen and nitrogen atoms being efficiently incorporated into highly functionalized, linear, and cyclic compounds.

The Neb-SOM contains several molecules of biological interest that have been detected in the SOM of primitive carbonaceous meteorites (e.g., hydroxy and carboxylic acids, urea, hydantoin, uracil, glycerol, and glycine derivatives; Sephton 2002; Pizzarello et al. 2006; Figure 2(A); Table 1).

Hydroxy acids detected in the Neb-SOM include lactic acid, 2-hydroxyisobutyric acid, and glycolic acid (Figure 2(A); Table 1). The conversion of glycolic acid, the smallest  $\alpha$ -hydroxy carboxylic acid, leads to the formation of glycine (Simakov et al. 2013), the simplest but crucial proteinaceous amino acid. Some of the lactic acid derivatives are intermediate species in autocatalytic pathways of reductive carbon assimilation from carbon oxides in complex organic structures of primordial metabolism (Morowitz et al. 2000). Note here that 2-methyl-propenoic acid identified in the Neb-IOM pyrolysate (Figure 2(B); Table 2) is the product of dehydration of the 2-hydroxyisobutyric acid, pointing to the presence of common structures in soluble and insoluble OM fractions.

Carbodiimide, the major compound of the Neb-SOM (Figure 2(A)), is a reactive condensing agent capable of assembling amino acids into peptides in liquid water (Hartmann et al. 1984). Moreover, carbodiimide is the stable isomer of cyanamide, an interstellar molecule and accepted prebiotic condensing agent that hydrolyzes into urea in liquid vapor (Duvernay et al. 2004) and that is the most abundant product of the pyrolysate of Neb-IOM (Figure 2(B)). The Neb-SOM also comprises urea (Figure 2(A); Table 1), a nitrogen-bearing basic component of living systems that is required for the phosphorylation of nucleosides under prebiotic conditions. In addition, because of its high polarity and dehydrating ability, molten urea allows the thermal polymerization of amino acids under prebiotic conditions to be made (Mita et al. 2005). Formyl urea is also released upon Neb-IOM pyrolysate (Figure 2(B); Table 2). Glycerol, which is detected in NEB-SOM (Figure 2(A); Table 1), was likely involved in the prebiotic formation of triacylglycerols, which possibly formed the first cell membranes within which the first biochemical reactions took place (Nuevo et al. 2010).

Uracil—the only pyrimidine-based nucleobase detected so far in carbonaceous meteorites (Pizzarello et al. 2006)—is detected in both Neb-SOM and Neb-IOM pyrolysate (Figure 2; Tables 1, 2). In Neb-SOM, it occurs along with dihydrouracil, 2,4-dihydropyrimidine (the enol form of uracil) and 2-hydroxy-4-amino-pyrimidine (the enol form of the nucleobase cytosine; Figure 2(A); Table 1). Dihydropyrimidinone, a related compound, is detected in NEB-IOM pyrolysate. Uracil and cytosine are ubiquitous as nucleobases in ribonucleic acids (RNA), and thus probably played a key role during the

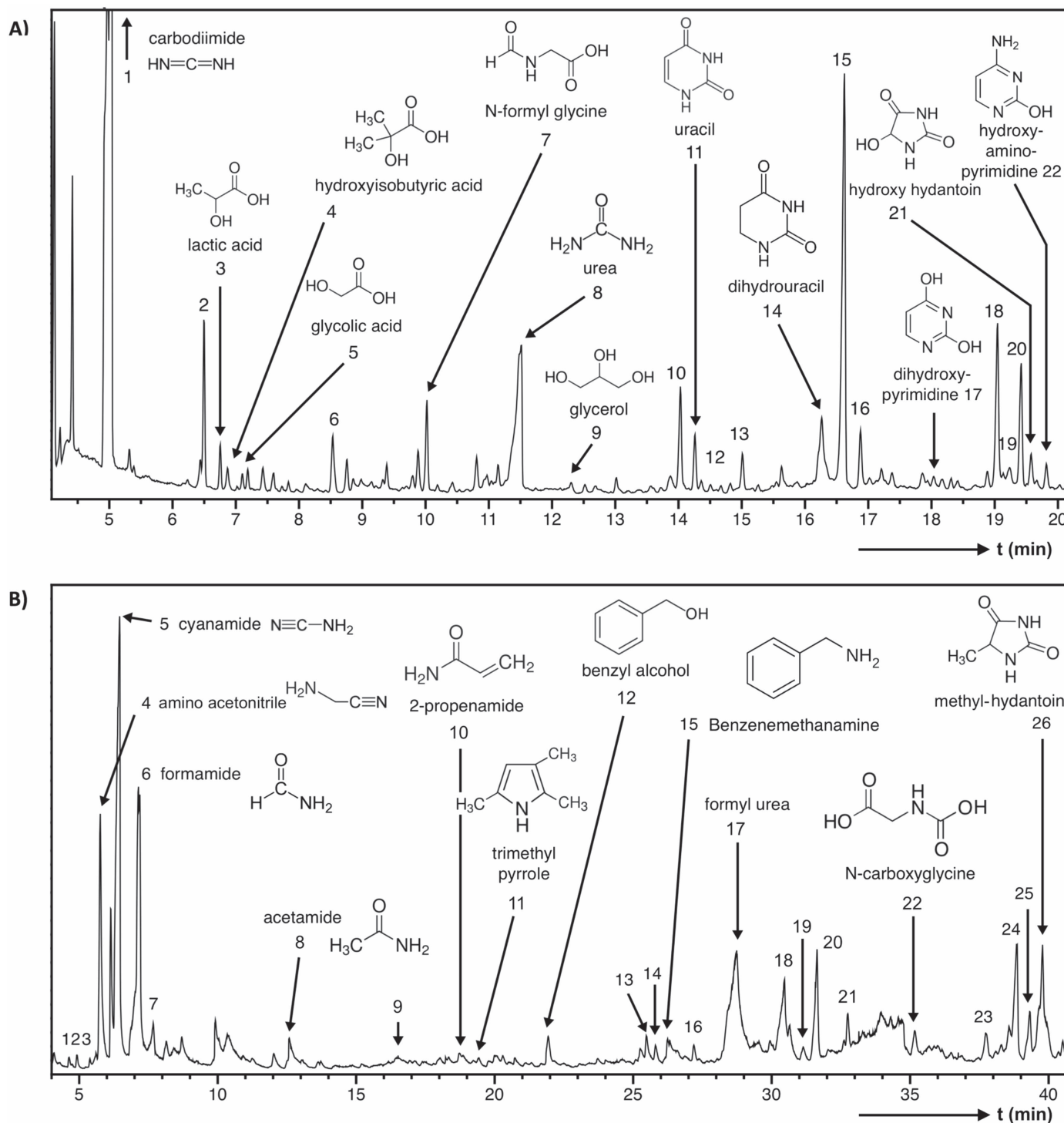


**Figure 2.** (A) GC-MS trace of the SOM extracted from the Nebultron organic condensate and derivatized using BSTFA. Numbers refer to Table 1. (B) GC-MS trace of pyrolysate of the IOM isolated from the Nebultron organic condensate in the presence of TMAH. Numbers refer to Table 2.

hypothesized “RNA world,” currently regarded as a primitive stage in the early evolution of life (Gilbert 1986).

5-hydroxy-2,4-imidazolidinedione and 1-methyl-2,4-imidazolidinedione, two derivatives of hydantoin, are also identified in the Neb-SOM and Neb-IOM pyrolysate, respectively (Figure 2, Tables 1, 2). Hydantoin, commonly formed by condensation of urea and glycolic acid, is of prime interest for prebiotic chemistry since it reacts upon hydrolysis to form carbamoyl amino acids, the precursors of N-carboxyanhydride

amino acids that can polymerize into poly- and oligopeptides (i.e., primitive proteins; Danger et al. 2006). Moreover, imidazolidinediones are typical pyrolysis products of protein amino acids in the presence of TMAH (Gallois et al. 2007). Finally, we report in the Neb-SOM the presence of N-formylglycine, which is known to yield glycine through hydrolysis (Bernstein et al. 2002). It must be noted that the oxidation product of this compound, N-carboxyglycine, is present in the pyrolysate of Neb-IOM, supporting again the

**Table 1**  
List of the Identified Compounds through GC–MS in the SOM Extracted from the Nebulotron Organic Condensate after Derivatization Using BSTFA

#	Mass	Ions	Molecule Detected
1	186	171, 73, 45, 78, 186	carbodiimide
2	188	115, 131, 73, 173, 43	4-hydroxy-4-methyl-2-pentanone
3	234	147, 73, 117, 191, 45, 133	lactic acid
4	248	147, 73, 131	2-hydroxyisobutyric acid
5	220	147, 73, 173, 205, 45	glycolic acid
6	?	156, 75, 73, 55, 43, 47	UC
7	247	73, 147, 188, 104, 204	N-formylglycine
8	204	147, 189, 73, 130, 171, 45, 52, 59, 87, 157	urea
9	308	73, 147, 205, 218, 133, 117, 103, 45	glycerol
10	?	73, 102, 117, 147, 131, 45	UC
11	256	241, 147, 99, 73, 255, 45, 113, 126, 59	uracil
12	255	240, 255, 147, 73, 45, 180	Pyrrole-2-carboxylic acid
13	?	73, 213, 129, 117, 45, 228	UC
14	258	243, 100, 73, 147, 59, 45, 258	dihydrouracil
15	?	229, 147, 73, 86, 100, 59, 45, 244	UC
16	?	100, 271, 73, 141, 256, 45	UC
17	256	73, 147, 256, 241, 100, 45	2, 4-dihydropyrimidine
18	255	73, 99, 100, 171, 241, 255	UC
19	246	75, 116, 131, 147, 231, 73, 45, 61	malonamide
20	270	73, 99, 100, 171, 255, 270	UC
21	332	147, 73, 317, 189, 202, 45, 174, 100, 117, 131	5-hydroxy-2,4-imidazolidinedione
22	255	240, 254, 73, 98, 170, 112, 45	2-hydroxy-4-amino-pyrimidine

**Note.** Note that the compounds occur as their silylated counterparts due to BSTFA derivatization. Numbers refer to the trace reported in Figure 1(A). UC: unidentified compound.

relationship between the two pools of synthesized OM. The early fermentation reaction of glycine could have provided a decisive energy source for primitive organisms (Clarke & Elsden 1980).

In addition to the products described above, the Neb-IOM pyrolysate also contains amides (formamide, acetamide, propanamide, and propenamide), heterocyclic nitrogenous compounds containing a pyrrole moiety (pyrrole, trimethylpyrrole), and aminoacetonitrile, which all present a biological interest (Figure 2(B); Table 2). Formamide, the simplest amide, is considered as the main building block in the origin of nucleic acids and could thus have been the starting point for prebiotic synthesis (Šponer et al. 2011). Acetamide is one among simple model molecules for the peptide linkage in polypeptides and proteins (Duvernay et al. 2004). This typical pyrolysis product from amino sugars has been detected on comet 67P/Churyumov–Gerasimenko (Goesmann et al. 2015). Moreover, malonamide, the amide of malonic acid was identified in the NEB-SOM (Figure 2(A); Table 1). Malonic acid, along with other small dicarboxylic acids, is a key compound in metabolic pathways. Pyrrole is notably formed upon pyrolysis of serine (Gallois et al. 2007). Moreover, it can further react with aldehydes to yield porphyrins (Chadha & Choughuley 1984), one of the best-known families of porphyrin metal complexes being heme, a cofactor of the protein hemoglobin. Note that the 1H-pyrrole-2-carboxylic acid identified in the Neb-SOM (Table 1) is closely linked to the amino acid (hydroxy)proline, the 2,5-dihydro-1H-pyrrole-2-carboxylic acid also being termed 3,4-Dehydro-DL-proline. Finally, aminoacetonitrile is a central molecule in the Strecker synthesis of glycine and is considered as one of the predominant ways to form amino acids in prebiotic environment and more especially in the Urey-Miller-type experiments (Miller 1996). Two compounds comprising a benzene ring and a functionalized substituent,

namely, benzyl alcohol and benzenemethanamine, also contribute to the Neb-IOM pyrolysate (Figure 2(B); Table 2).

## 5. Astrophysical Relevance

### 5.1. High-temperature Organosynthesis in the Photosphere of the PSN

These results demonstrate that electron-driven chemical reactions within radical-rich plasma environments in the PPD could supply biologically relevant molecules to the building blocks of asteroids and thus contribute to the molecular diversity of the SOM in carbonaceous chondrites (Botta & Bada 2002; Schmitt-Kopplin et al. 2010). However, pyrolysis of carbonaceous chondrite IOM yields a poorly functionalized assemblage of aromatic compounds (Remusat et al. 2005) that differs from the molecular composition reported in this study for the Neb-IOM. This indicates that either the IOM synthesized in the gas phase of the disk was subject to secondary processing accounting for its evolution toward a chondritic-like composition, or that an alternative synthesis route is at the origin of the IOM of primitive meteorites (Figure 3). For instance, the thermal alteration of organic matter is known to be associated with a step of carbonization (in the 100–500°C temperature range), which is characterized by chemical changes starting with the loss of labile chemical groups containing heteroelements (O, N) followed by that of aliphatic units, resulting in the relative enrichment in aromatic structures (aromatization; Alexander et al. 2007). Likewise, part of the biomolecules detected here in the Neb-IOM may be made soluble only during parent body aqueous alteration and secondary processing (Herd et al. 2011). While the SOM component of primitive meteorites would correspond to a pristine and undisturbed component, their IOM may partly originate from the photo- and thermo-processing of organic precursors (De Marcellus et al. 2016). Once formed in the

**Table 2**

List of the Identified Compounds through Pyrolysis GC–MS in the Presence of TMAH in the IOM Extracted from the Nebulotron Organic Condensate

#	Mass	Ions	Molecule Detected
1	100	41, 69, 39, 100, 85,	2-methyl-propenoic acid
2	102	43, 74, 71, 55, 59, 87	butanoic acid
3	81	81, 80, 39, 53, 42, 78, 82	1H-Pyrrole
4	84	83, 84, 58, 42, 40, 43, 57	aminoacetonitrile
5	70	69, 70, 42, 53, 71, 67	cyanamide
6	73	73, 44, 42, 43, 45, 41, 56, 58, 72, 74	formamide
7	?	58, 74, 89	UC
8	87	44, 87, 72, 43, 45, 42	Acetamide
9	87	58, 87, 57, 86, 88, 59, 42	propanamide
10	99	98, 55, 44, 58, 72, 99	2-propenamamide
11	109	108, 109, 94, 67, 42	2,3,5-trimethyl-1H-pyrrole
12	122	91, 122, 121, 77, 65, 51, 39	Benzyl alcohol
13	?	125, 40, 68, 39, 96, 58	UC
14	146	115, 55, 59, 87, 45, 114	UC
15	135	58, 91, 134, 135, 42, 44, 65, 77	benzenemethanamine
16	111	111, 82, 55, 42, 56, 68	2,3-dihydro-4(1H)-pyrimidinone
17	130	44, 72, 102, 58, 42, 45	formyl urea
18	?	113, 56, 58, 85	UC
19	?	56, 140, 42, 112, 83, 69	UC
20	?	42, 127, 58, 70	UC
21	?	139, 54, 39, 82, 58, 110, 124	UC
22	161	102, 58, 42, 59, 130, 161	N-carboxyglycine
23	?	42, 127, 98, 70, 55, 138, 153	UC
24	?	128, 42,43, 100, 70, 56, 136	UC
25	140	140, 55, 83, 54, 70, 40, 111, 82,	uracil
26	142	42, 127, 142, 56, 57, 58, 70, 99	1-methyl-2,4-imidazolidinedione

**Note.** Note that the compounds occur as their methylated counterparts due to TMAH. Numbers refer to the trace reported in Figure 1(B). UC: unidentified compound.

photosphere of the disk, organic material interaction with soft X-rays and/or ionized molecules ( $\text{H}_2\text{D}^+$ ; Robert et al. 2011) could lead to the deuterium enrichments observed in extra-terrestrial organic matter. These results indicate that part of the biomolecules detected in the SOM of primitive meteorites could have been synthesized in the photosphere of the PSN, but that a unique environment/mechanism of organosynthesis may not account for both the SOM and IOM observed in meteorites. A similar conclusion was reached from pyrolytic and spectroscopic studies of the IOM and SOM from Orgueil and Murchison carbonaceous chondrites (Remusat et al. 2005).

Importantly, chondritic noble gases are intimately associated with the IOM in meteorites, likely pointing to a common and pre-asteroidal accretion origin. It is demonstrated that ionizing conditions were required for the chondritic noble gas isotopes to be efficiently incorporated in organic materials and fractionated as systematically observed in chondrites (Marrocchi et al. 2011; Kuga et al. 2015). This suggests that the IOM of meteorites is mainly formed within organic-radical-rich environments of the PSN, as attested by the macromolecular structure of the IOM isolated from Murchison meteorite (Derenne & Robert 2010).

Based on previous Nebulotron experiments (Kuga et al. 2015), we conclude that radical-rich environments in the PSN probably supplied most of the chondritic IOM, and could also have supplied part of the biomolecules observed in comets and meteorites. However, it is not yet possible to discriminate the exact conditions (e.g., redox) that led to the synthesis of organic molecules in the photosphere of the disk. The respective contributions of radicals, ions, and neutral species, as well as the possible role of catalysts (e.g., grain surfaces) in the chemical reaction leading to the formation of organic molecules in the gas phase of the PSN are not unraveled. The photosphere of the disk contains the highest concentrations in both ionized species and radicals within the disk, and therefore, regardless of the exact nature of the dominating reagents (ions, radicals, and/or neutral species), constitutes the more likely environment for organosynthesis to occur.

Ionization sources in PPDs are multiple (UV photons from parent T-Tauri stars, X-rays, and excess UV photons from accretion shocks and lightning, interstellar UV photons and cosmic rays, radioactive decays of  $^{26}\text{Al}$  and  $^{40}\text{K}$  isotopes, thermal excitation in the hot zones), making the synthesis of organic molecules potentially ubiquitous in the PSN (Figure 3). The synthesis of organic compounds, including biomolecules, in the PSN would be the most effective in the disk's photosphere, where the degrees of ionization, fractional abundances of electrons, and organic radical densities are the most elevated (Walsh et al. 2012; Robert et al. 2017). This does not, however, preclude other pathways of biomolecule synthesis in the ISM (Nuevo 2011) or during asteroidal aqueous alteration (Kebukawa et al. 2017; Figure 3), but indicates that meteoritic and cometary biomolecules were possibly supplied from radical-rich plasma environments in the PSN. The different synthesis routes of organic materials in the PSN are summarized in Figure 3. By analogy with the outward transport of crystalline silicates to the region of long-period comet formation (Bockelée-Morvan et al. 2002), organic materials synthesized in the solar nebula—e.g., formamide, glycine—could have been efficiently transported outward by turbulent motion or by bipolar outflows to the regions where they are now detected in comets. Infrared observations of classical T-Tauri stars demonstrate that simple molecules (e.g.,  $\text{CO}_2$ ,  $\text{HCN}$ ,  $\text{C}_2\text{H}_2$ ) are common in protostellar nebulae and that the gas temperatures (200–800 K) and emitting areas are consistent with the emission originating in a warm disk atmosphere (Carr & Najita 2011). Reaction rates of the various chemical processes at stake in the Nebulotron experiment would likely be smaller in the effective photosphere of the PSN where  $\text{H}_2$  and He largely dominate the gas composition (Iro et al. 2003) and the gas pressure is  $<1$  mbar (Walsh et al. 2010). The photon-dominated region (PDR; with gas temperatures of a few thousand K) is almost fully ionized (Glassgold et al. 2004; Woitke 2015). The underlying warm molecular layer (WML; with gas temperatures  $\leq 1000$  K) is also largely ionized but with a mean lifetime of organic molecules being much longer than in the PDR. The WML has a very active chemistry and is mainly responsible for the observable line emissions in the near-IR and mid-IR (Woitke 2015). These two layers of the disk constitute here the so-called photosphere of the PSN (Figure 3). The high temperature of neutral gas in the Nebulotron plasma (800–1000 K) is mostly relevant to thermal conditions expected for the WML of the disk where organosynthesis takes place (Glassgold et al. 2004; Figure 3).

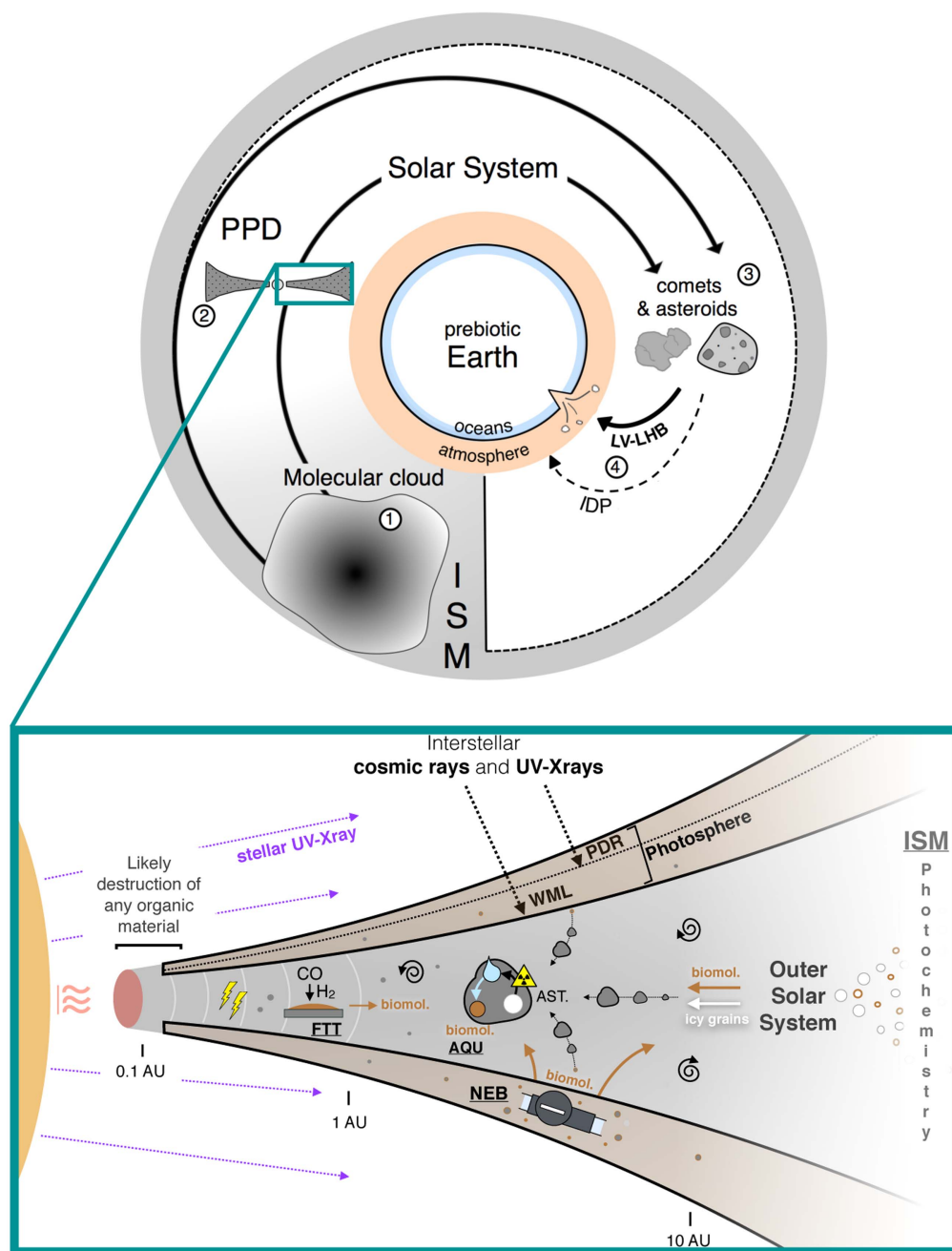


**Figure 3.** Possible exogenous sources of organic molecules on prebiotic Earth. Interstellar materials are either unprocessed by the PPD phase and directly incorporated into cometary bodies, or processed by the PPD phase and incorporated into comets and asteroids. Both comets and asteroids were supplied to the early Earth during the final building stages of the Earth (Late Vener episode, LV, or, more probably, Late Heavy Bombardment, LHB; Marty et al. 2016). Subsequent and continuous addition through the continuous infall of interplanetary dust particles (IDPs) is also considered (Whittet 1997). The zoomed-in section highlights the principal routes of extraterrestrial biomolecule synthesis/processing in the PSN. FTT: Fischer–Tropsch-type (FTT) catalytic reduction of CO by hydrogen (Hayatsu et al. 1971; Nuth et al. 2008). Thunderbolts refer to processes of organosynthesis induced by spark discharges (Wolman et al. 1972; Desch & Cuzzi 2000). The melting of accreted ice upon radioactive heating may induce processes of organosynthesis during aqueous alteration (AQU) of asteroids (AST; Kopetzki & Antonietti 2011; Kebukawa et al. 2017). NEB refers to the Nebultron experiments, with a high-temperature organosynthesis upon irradiation in the photosphere (i.e., photon-dominated region, PDR, and Warm Molecular Layer, WML; Kuga et al. 2015) of the PSN (this study). Nebular organic materials and biomolecules (including supplies from the ISM) would be widely distributed in PPDs through turbulent diffusion (depicted as whirls), thus pointing to a complex origin of the extraterrestrial organics that were delivered to prebiotic Earth.

In this region, the gas temperature is thought to be higher than that of the grains (Walsh et al. 2010; Woitke 2015). The temperature of the surface of the quartz tube reactor in the Nebultron experiment, also lower ( $\sim 500$  K) than that of the gas, might therefore be considered as analogous to the surface of solid particles lofted to the WML by turbulent diffusion (see Section 5.2).

The irradiation of an achiral ice mixture with circularly polarized light in the UV range has successfully produced amino acids with enantiomeric excesses proportional to the number of polarized photons and of opposite signs with respect to light polarization (De Marcellus et al. 2011). This latter point brings a possible explanation to the longstanding issue of the origin of biomolecules laevo-rotatory (L) amino acids

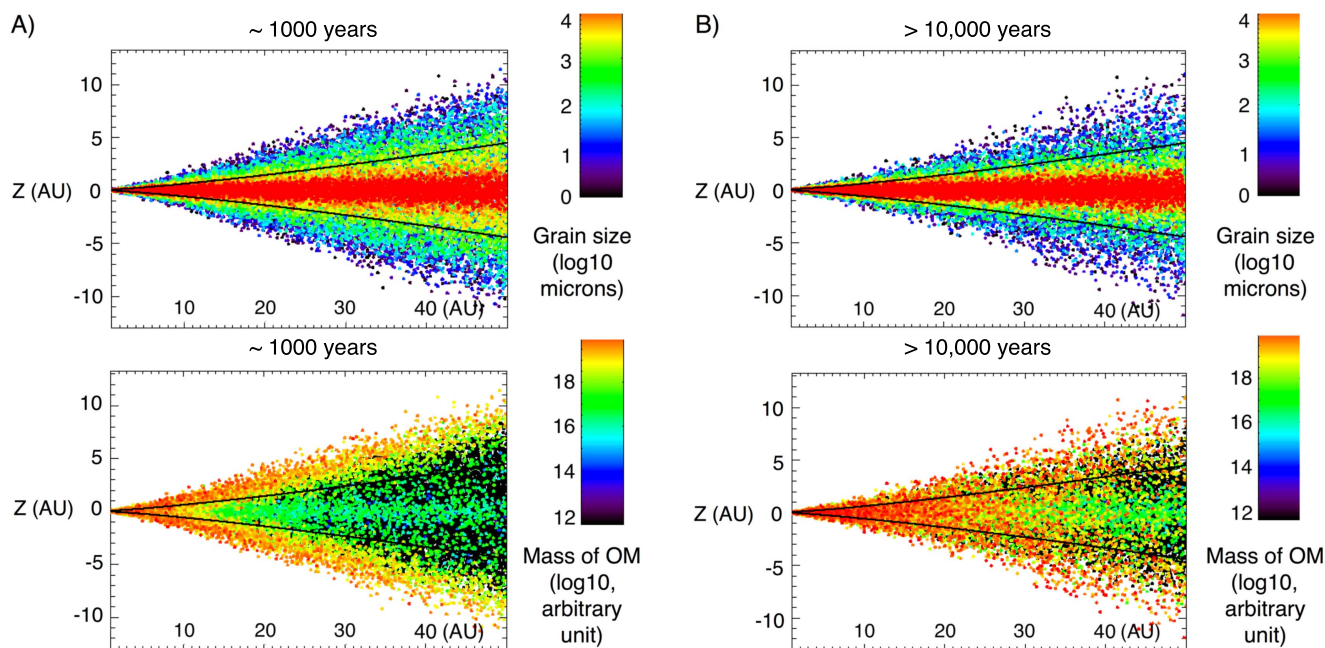


**Figure 4.** Grain size and mass distribution of organic materials in the disk, after  $\sim 1000$  years (A) and  $> 10,000$  years (B) of numerical simulation. The solid horizontal lines show the location of the pressure scale height ( $H$ ; Charnoz et al. 2011). The grain size distribution clearly shows the sedimentation process, with small particles being widely spread vertically, whereas big particles sediment rapidly and gather close to the midplane ( $z = 0$ ). Small particles are coupled with the turbulent motion of the gas and are therefore continuously lofted to the photosphere of the disk (taken over  $2 \times H$ ) where organosynthesis occurs. Initial content of organic matter:  $10^{-14} \text{ kg m}^{-3}$ . Production rate in the photosphere:  $10^{-18} \text{ kg m}^{-2} \text{ s}^{-1}$ .

homochirality in living systems. In this scenario, exogenous organics displaying slight L excess (Pizzarello et al. 2006) would have been delivered to early Earth, thus transferring their asymmetry to the prebiotic building blocks of life (Figure 3). While chiral excesses would be hard to generate in the context of liquid-water reactions on meteorite parent bodies or FTT reactions, biomolecule synthesis within the irradiated environments of the disk provides an alternative pathway for the formation of molecules relevant to life in space and opens a promising avenue of investigation for achiral chemistry upon irradiation in the PSN photosphere. Analyzing organic materials synthesized in the high-vacuum Nebulotron plasma setting for their nitrogen and hydrogen isotopes might also provide a test to extrapolate experimental results to some natural environments. The fact that nitrogen trapped in organics produced during plasma organosynthesis does not reproduce the  $^{15}\text{N}$  enrichments observed in meteorites IOM (Kuga et al. 2014), whereas some H isotope anomalies are reproduced (Robert et al. 2017) is consistent with D/H versus  $^{15}\text{N}/^{14}\text{N}$  variations in meteoritic organics (Aléon 2010), potentially pointing to different isotope fractionation mechanisms for H and N in the PSN.

### 5.2. LIDT3D Code and Turbulent Diffusion of Organic Materials in the Disk

The turbulent diffusion of dust grains subject to gravitational settling, radial drift, and turbulent diffusion in a PPD has been investigated by a stochastic and physically justified procedure developed by Charnoz et al. (2011) and Charnoz & Taillifet (2012). Our simple approach, based on this numerical model of dust transport, predicts the general outlines of the transport of organic materials—including biomolecules—synthesized in the photosphere of the disk and investigates their relationship with dust grains (see Section 2.5).

Figures 4(A)–(B) display both the grain size distribution and the repartition of organic materials in the disk, after  $\sim 1000$  years and  $> 10,000$  years evolution, respectively. At  $\sim 1000$  years, we observe a sedimentation process, with the largest particles already settling to the midplane (in red;  $z = 0$ ), while smaller particles are distributed over the height of the disk because of their diffusion due to the turbulent motion of the gas (Charnoz et al. 2011). The fraction of organic matter present at the midplane (in green; Figure 4(A)), associated with the larger particles of the disk, would experience little exposure to irradiation in the photosphere and, thus, would remain preserved as pristine material. These materials would rapidly be incorporated into the first planetary bodies forming at the midplane after inward drift. In contrast, the fraction of organic matter present in the upper layers of the disk (in red; Figure 4(A)) is associated with the particles of smaller sizes. The motion of small dust particles is tightly coupled to that of the gas (Charnoz et al. 2011). Hence, small grains are preferentially lofted by turbulent diffusion to the photosphere of the disk where organosynthesis occurs. In addition, they have high surface/volume ratios, thus maximizing the amount of organic materials possibly trapped at the surface of dust particles. Organic materials covering the surface of silicate grains would likely enhance their sticking efficiency (Kouchi et al. 2002). This would result in increased grain coagulation rates, thus favoring conditions that trigger streaming instabilities (Bai & Stone 2010; Drażkowska & Dullemond 2014) and an enhanced growth of macroscopic bodies such as planetesimals or future asteroids (Kouchi et al. 2002; Figure 3). Such a transport of newly formed organic materials (including biomolecules) from the irradiated and hot regions of the disk, where they are synthesized, to shielded parts of the midplane would ensure their efficient preservation in meteorite parent bodies, and would account for the intimate association of

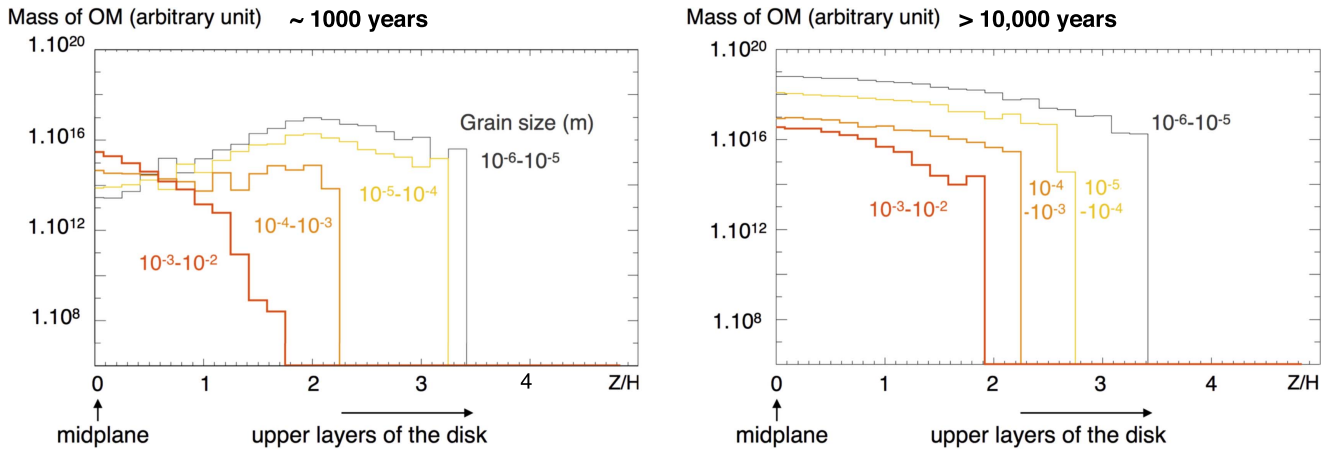


**Figure 5.** Vertical distribution of the OM as a function of the size category and vertical position of the particles integrated from 7 to 50 au (i.e., over the radius of the disk except the dead zone). The vertical position is given as the actual height ( $Z$ ) normalized to the pressure height scale at the corresponding radius ( $Z/H$  ratio). The picture is displayed at  $\sim 1000$  years and more than 10,000 years of numerical simulation. Initial content of organic matter:  $10^{-14} \text{ kg m}^{-3}$ . Production rate in the photosphere:  $10^{-18} \text{ kg m}^{-2} \text{ s}^{-1}$ .

meteoritic organic matter and silicates as observed in meteorites (Zega et al. 2010).

In Figure 4(B) ( $> 10,000$  years), we observe that the fraction of organic matter associated with the smaller particles (in red) is progressively distributed in the PPD by turbulent diffusion and gas drag. Organic materials synthesized in the photosphere of the disk could thus potentially represent precursors of meteoritic and cometary organics, before their thermal/photoprocessing and subsequent modification by secondary parent body processing. The coupled effect of gas drag and turbulent diffusion induces an inward transport of dust in the disk’s midplane where the disk is sub-Keplerian toward the region of planetesimal formation, while favoring outward transport (toward the comet formation region) in the disk’s upper layers (Charnoz et al. 2011) where the disk is super-Keplerian.

The same conclusions can be drawn from the analysis of Figure 5, which displays the distribution of the OM as a function of the size and vertical position of the particles integrated from 7 to 50 au (i.e., over the radius of the disk except the dead zone). The vertical position is given as the actual height ( $Z$ ) normalized to the pressure height scale at the corresponding radius ( $Z/H$  ratio). We observe that, whereas large particles dominate the budget of organic matter close to the midplane at  $\sim 1000$  years, small particles dominate this budget after 10,000 years of simulation. This is due to the fact that small particles are continuously lofted to the photosphere of the disk where organosynthesis occurs. They accumulate more and more organic materials and keep being transported throughout the disk—including to the midplane—by turbulent diffusion (Figure 3). Note that alternative pathways of organic matter synthesis (Figure 3) may be effective in the deeper layers of the disk (e.g., FTT reactions, asteroidal aqueous alteration that may occur at later times), but are not modeled here, the main point of this discussion being to track the transport of organic materials synthesized in the photosphere of the PSN.

As depicted in Section 2.5, defining absolute production rates for organic materials synthesized in the photosphere of the PSN is extremely difficult. Here, our a priori approach based on arbitrary production rates allows the general sketch of the transport of organic materials synthesized in the photosphere of

the disk to be evaluated. Interestingly, the possibility that the disk is mostly laminar in its midplane (Inutsuka & Sano 2005; Okuzumi & Hirose 2011) and very turbulent in its upper layers (see, e.g., Schnepf et al. 2015) is heavily debated. An almost laminar midplane ( $\alpha \sim 10^{-4}$ ) would promote coagulation as a result of lower encounter velocities between particles. In the case of a PPD containing a dead zone, it has been shown that coagulation processes rapidly produce big particles, up to 10 cm in size, close to the disk’s midplane (Charnoz & Taillifet 2012). Here, grain size evolution through fragmentation or coagulation could not be taken into account since it would have drastically complicated the tracking of individual super-particles content of organic matter. We note that the effect of a dead zone mainly affects the largest grains ( $> 0.1$  mm in size; Charnoz & Taillifet 2012), which are not the main carriers of organic materials in our simulations (Figures 4–5). We find that organic materials synthesized in the photosphere of the PSN would likely be associated with small dust particles, which are coupled to the motion of the gas and therefore preferentially lofted to the upper layers of the disk where organosynthesis occurs. Larger particles would likely settle at the midplane before experiencing inward radial drift and being trapped in the dead zone where enhanced particle growth occurs (Charnoz & Taillifet 2012). According to our model, in the case of low production rates in the photosphere of the disk, most of the organic matter present in the disk would correspond to materials inherited from alternative processes of organosynthesis, distributed in volume within the particles (Figure 3). In this case, the dead zone, which concentrates the largest particles, would be enriched in organic materials relative to the rest of the disk (Figure 6(A)). In the case of high organic matter production rates in the photosphere relative to the content of organic materials distributed in volume within particles and inherited from alternative processes of organosynthesis (Figure 6(B)), organic materials are mostly associated with the smallest grains, which are spread out within the disk by turbulent diffusion and little affected by the presence of the dead zone. Over the lifetime of the disk, the gas phase is expected to progressively dissipate (which is not simulated here using the LIDT3D code because of mass conservation), thus allowing the smaller particles to definitively settle at the midplane and be incorporated in the planetary bodies. If freely

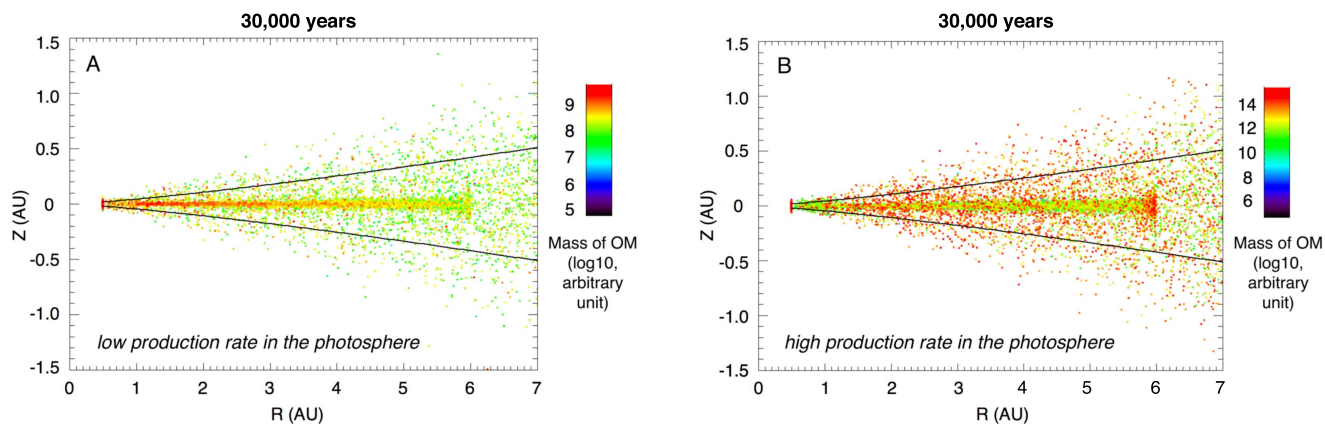


**Figure 6.** Mass distribution of organic materials in the inner part of the disk, where a dead zone is present (from 1 to 6 au), after 30,000 years of numerical simulation, in case of low (A) and high (B) organic matter production rates in the photosphere. The initial budget of organic matter of each grain (proportional to the volume of the particle and taken as a proxy of the potential inheritance from alternative processes of organosynthesis; Figure 3) is the same for both simulations. The solid horizontal lines show the location of the pressure scale height ( $H$ ; Charnoz et al. 2011). Initial content of organic matter:  $10^{-14}$  kg m $^{-3}$  for (A)–(B). Production rate in the photosphere:  $10^{-26}$  kg m $^{-2}$  s $^{-1}$  (A) and  $10^{-20}$  kg m $^{-2}$  s $^{-1}$  (B).

transported in the gas phase and not trapped at the surface of silicate grains, organic globules as synthesized in the reaction chamber of the Nebulotron ( $\sim 1$   $\mu$ m in size; Figure 2) would experience a wide transport within the PPD, by analogy with the random and extensive trajectories of  $\mu$ m-sized particles subject to turbulent diffusion in the PSN (Charnoz et al. 2011; Figure 3). Organic globules synthesized in the photosphere of the PSN could thus represent precursors of the globules observed in carbonaceous chondrite meteorites and IDPs (De Gregorio et al. 2010).

It should be noted that the gas disk considered in this paper is a simple, turbulently active, and non-evolving parameterized gaseous disk (Takeuchi & Lin 2002; Charnoz et al. 2011) that has been chosen for the sake of simplicity. Very short timescales (on the order of tens of thousand years) were sufficient to derive the general sketch of such a transport. The total amount of organic materials present in the disk increased linearly with time after only a few thousand years, following the same trend of organic matter spatial distribution as described in this paper. Note that the diffusion time of particles from the photosphere of the disk (at  $z = 2H$ ) to the midplane (at  $z = 0$ ) is given by  $(2H)^2/D_d$ , with  $D_d$  the dust diffusion coefficient given calculated as  $D_d \sim \alpha CsH/Sc$ , where  $Cs$  is the local sound velocity and  $Sc$  is the Schmidt coefficient tending to 1 in the limit of very small particles and increasing to infinity for large particles (Youdin & Lithwick 2007). According to our model, the diffusion time of small particles ( $\propto 1/\alpha$ ) would thus increase by two orders of magnitude for a disk with an  $\alpha$  parameter set at  $10^{-4}$  instead of  $10^{-2}$ . Grain size evolution through coagulation, which has not been taken into account here, should play an important role in the transport of newly formed organic materials (including biomolecules) from the irradiated and hot regions of the disk, where they are synthesized, to shielded parts of the midplane where they would be preserved in meteorite parent bodies.

## 6. Conclusion

A high-vacuum plasma setting was designed to produce organic condensates from a high purity gas phase reminiscent of the irradiated environments in the PSN. Recovered

materials exhibit a large range of biomolecules, including amino acid and nucleobase derivatives, which have been detected in meteorites and are expected to have played a key role in the emergence of life on prebiotic Earth. This finding does not preclude other pathways of biomolecules synthesis in the ISM and/or during asteroidal aqueous alteration but indicates that processes of biomolecule synthesis could have been also effective in the hot and ionized photosphere of the PSN. The apparent extensive radial mixing that occurred in the early solar system and the multiple potential sources of organics and biomolecules in the inner solar system (e.g., inward contribution of interstellar/cometary organics, high-temperature synthesis in the photosphere or FTT reactions in the PSN, aqueous alteration of organic materials onto meteorite parent bodies) point to a complex origin of the extraterrestrial organic matter and biomolecules that were delivered to prebiotic Earth.

Laurette Piani and Michael Broadley are thanked for participating in fruitful discussions. We thank Delphine Lequin for technical assistance. We gratefully acknowledge the two anonymous reviewers and the Editor for their constructive comments. This study was supported by the European Research Council (PHOTONIS project, grant agreement No. 695618 to B.M.). This is CRPG-CNRS contribution 2587. Author contributions: D.B., Y.M., L.T., and B.M. participated in designing and building the high-vacuum Nebulotron. D.B. did the organic synthesis and recovery from the discharge tube. D.B., S.D., and C.A. performed the soluble organic matter (SOM)—insoluble organic matter (IOM) separation and analyses by GC–MS and Curie point pyrolysis GC–MS (Py GC–MS). D.B. and S.C. did the numerical simulations. All the authors discussed the results and their interpretations. D.B., Y.M., B.M., S.D., and S.C. wrote the manuscript. The authors declare no competing financial interests.

## ORCID iDs

David V. Bekaert <https://orcid.org/0000-0002-1062-6221>  
 Yves Marrocchi <https://orcid.org/0000-0001-7075-3698>  
 Sebastien Charnoz <https://orcid.org/0000-0002-7442-491X>  
 Bernard Marty <https://orcid.org/0000-0001-7936-1519>

## References

- Aléon, J. 2010, *ApJ*, **722**, 1342
- Alexander, C. O. D., Fogel, M., Yabuta, H., & Cody, G. D. 2007, *GeCoA*, **71**, 4380
- Altwegg, K., Balsiger, H., Bar-Nun, A., et al. 2016, *SciA*, **2**, e1600285
- Bai, X. N., & Stone, J. M. 2010, *ApJ*, **722**, 1437
- Baillie, K., & Charnoz, S. 2014, *A&A*, **786**, 35
- Bernstein, M. P., Dworkin, J. P., Sandford, S. A., Cooper, G. W., & Allamandola, L. J. 2002, *Natur*, **416**, 401
- Birnstiel, T., Dullemond, C. P., & Brauer, F. 2010, *A&A*, **513**, A79
- Biron, K., Derenne, S., Robert, F., & Rouzaud, J. N. 2015, *M&PS*, **50**, 1408
- Bockelée-Morvan, D., Gautier, D., Hersant, F., Huré, J. M., & Robert, F. 2002, *A&A*, **384**, 1107
- Botta, O., & Bada, J. L. 2002, *SGeo*, **23**, 411
- Capaccioni, F., Coradini, A., Filacchione, G., et al. 2015, *Sci*, **347**, aaa0628
- Carr, J. S., & Najita, J. R. 2011, *ApJ*, **733**, 102
- Chadha, M. S., & Choughuley, A. S. U. 1984, *OrLi*, **14**, 469
- Chakraborty, S., Ahmed, M., Jackson, T. L., & Thiemens, M. H. 2008, *Sci*, **321**, 1328
- Chakraborty, S., Muskatel, B. H., Jackson, T. L., et al. 2014, *PNAS*, **111**, 14704
- Charnoz, S., Aléon, J., Chaumard, N., Baillié, K., & Taillifet, E. 2015, *Icar*, **252**, 440
- Charnoz, S., Fouchet, L., Aléon, J., & Moreira, M. 2011, *ApJ*, **737**, 33
- Charnoz, S., & Taillifet, E. 2012, *ApJ*, **753**, 119
- Chyba, C., & Sagan, C. 1992, *Natur*, **355**, 125
- Ciesla, F. J. 2006, *ApJL*, **654**, L159
- Clarke, P. H., & Elsdén, S. R. 1980, *JMoIE*, **15**, 333
- Danger, G., Boiteau, L., Cottet, H., & Pascal, R. 2006, *JChS*, **128**, 7412
- De Gregorio, B. T., Stroud, R. M., Nittler, L. R., et al. 2010, *GeCoA*, **74**, 4454
- De Marcellus, P., Fresneau, A., Brunetto, R., et al. 2016, *MNRAS*, **464**, 114
- De Marcellus, P., Meinert, C., Nuevo, M., et al. 2011, *ApJL*, **727**, L27
- Derenne, S., & Robert, F. 2010, *M&PS*, **45**, 1461
- Desch, S. J., & Cuzzi, J. N. 2000, *Icar*, **143**, 87
- Drążkowska, J., & Dullemond, C. P. 2014, *A&A*, **572**, A78
- Duvernay, F., Chiavassa, T., Borget, F., & Aycard, J. P. 2004, *JChS*, **126**, 7772
- Elsila, J. E., Glavin, D. P., & Dworkin, J. P. 2009, *M&PS*, **44**, 1323
- Fomenkova, M. N., Chang, S., & Mukhin, L. M. 1994, *GeCoA*, **58**, 4503
- Fromang, S., & Papaloizou, J. 2006, *A&A*, **452**, 751
- Fromang, S., Terquem, C., & Balbus, S. A. 2002, *MNRAS*, **329**, 18
- Gallois, N., Templier, J., & Derenne, S. 2007, *J. Anal. Appl. Phys.*, **80**, 216
- Gilbert, W. 1986, *Natur*, **319**, 618
- Glassgold, A. E., Najita, J., & Igea, J. 2004, *ApJ*, **615**, 972
- Goesmann, F., Rosenbauer, H., Bredehöft, J. H., et al. 2015, *Sci*, **349**, aab0689
- Hartmann, J., Nawroth, T., & Dose, K. 1984, *OLEB*, **14**, 213
- Hayatsu, R., Studier, M. H., & Anders, E. 1971, *GeCoA*, **35**, 939
- Herd, C. D., Blinova, A., Simkus, D. N., et al. 2011, *Sci*, **332**, 1304
- Hollis, J. M., Lovas, F. J., & Jewell, P. R. 2000, *ApJL*, **540**, L107
- Inutsuka, S. I., & Sano, T. 2005, *ApJL*, **628**, L155
- Iro, N., Gautier, D., Hersant, F., Bockelée-Morvan, D., & Lunine, J. I. 2003, *Icar*, **161**, 511
- Kebukawa, Y., Chan, Q. H., Tachibana, S., Kobayashi, K., & Zolensky, M. E. 2017, *SciA*, **3**, e1602093
- Kopetzki, D., & Antonietti, M. 2011, *New J. Chem.*, **35**, 1787
- Kouchi, A., Kudo, T., Nakano, H., et al. 2002, *ApJL*, **566**, L121
- Kuga, M., Carrasco, N., Marty, B., et al. 2014, *E&PSL*, **393**, 2
- Kuga, M., Cernogora, G., Marrocchi, Y., Tissandier, L., & Marty, B. 2017, *GeCoA*, **217**, 219
- Kuga, M., Marty, B., Marrocchi, Y., & Tissandier, L. 2015, *PNAS*, **112**, 7129
- Marrocchi, Y., Marty, B., Reinhardt, P., & Robert, F. 2011, *GeCoA*, **75**, 6255
- Marty, B., Avice, G., Sano, Y., et al. 2016, *E&PSL*, **441**, 91
- Miller, S. L. 1996, *OLEB*, **26**, 201
- Mita, H., Nomoto, S., Terasaki, M., Shimoyama, A., & Yamamoto, Y. 2005, *IJAsB*, **4**, 145
- Morowitz, H. J., Kostelnik, J. D., Yang, J., & Cody, G. D. 2000, *PNAS*, **97**, 7704
- Muskatel, B. H., Remacle, F., Thiemens, M. H., & Levine, R. D. 2011, *PNAS*, **108**, 6020
- Nuevo, M. 2011, in Proc. Frank N. Bash Symp., New Horizons in Astronomy, ed. S. Salviander, J. Green, & A. Pawlik (Trieste: SISSA), 004, <https://pos.sissa.it/149/004/>
- Nuevo, M., Bredehöft, J. H., Meierhenrich, U. J., d'Hendecourt, L., & Thiemann, W. H. P. 2010, *AsBio*, **10**, 245
- Nuth, J. A., III, Johnson, N. M., & Manning, S. 2008, *ApJL*, **673**, L225
- Okuzumi, S., & Hirose, S. 2011, *ApJ*, **742**, 65
- Pizzarello, S., Cooper, G. W., & Flynn, G. J. 2006, in Meteorites and the Early Solar System II, Vol. 1, ed. D. S. Lauretta & H. Y. McSween, Jr. (Tucson, AZ: Univ. Arizona Press), 625
- Remusat, L., Derenne, S., Robert, F., & Knicker, H. 2005, *GeCoA*, **69**, 3919
- Robert, F., Derenne, S., Lombardi, G., et al. 2017, *PNAS*, **114**, 870
- Robert, F., Derenne, S., Thomen, A., Anquetil, C., & Hassouni, K. 2011, *GeCoA*, **75**, 7522
- Saito, M., & Kimura, Y. 2009, *ApJL*, **703**, L147
- Schmitt-Kopplin, P., Gabelica, Z., Gougeon, R. D., et al. 2010, *PNAS*, **107**, 2763
- Schnepf, N. R., Lovelace, R. V., Romanova, M. M., & Airapetian, V. S. 2015, *MNRAS*, **448**, 1628
- Sephton, M. A. 2002, *Nat. Prod. Rep.*, **19**, 292
- Shock, E. L., & Schulte, M. D. 1990, *Natur*, **343**, 728
- Sicilia-Aguilar, A., Henning, T., Dullemond, C. P., et al. 2011, *ApJ*, **742**, 39
- Simakov, A., Miller, G. B., Bunkan, A. J., Hoffmann, M. R., & Uggerud, E. 2013, *PCCP*, **15**, 16615
- Snyder, L. E., Lovas, F. J., Hollis, J. M., et al. 2005, *ApJ*, **619**, 914
- Šponer, J. E., Mládek, A., Šponer, J., & Fuentes-Cabrera, M. 2011, *JPCA*, **116**, 720
- Taillifet, E., Baillié, K., Charnoz, S., & Aléon, J. 2014, in LPSC, **45**, 2086
- Takeuchi, T., & Lin, D. N. C. 2002, *ApJ*, **581**, 1344
- Vinogradoff, V., Bernard, S., Le Guillou, C., & Remusat, L. 2017, *Icar*, **305**, 358
- Visser, R., Van Dishoeck, E. F., & Black, J. H. 2009, *A&A*, **503**, 323
- Walsh, C., Millar, T. J., & Nomura, H. 2010, *ApJ*, **722**, 1607
- Walsh, C., Nomura, H., Millar, T. J., & Aikawa, Y. 2012, *ApJ*, **747**, 114
- Whittet, D. C. B. 1997, in Planetary and Interstellar Processes Relevant to the Origins of Life (Netherlands: Springer), 249
- Woitke, P. 2015, *EPJWC*, **102**, 00011
- Wolman, Y., Haverland, W. J., & Miller, S. L. 1972, *PNAS*, **69**, 809
- Youdin, A. N., & Lithwick, Y. 2007, *Icar*, **192**, 588
- Zega, T. J., Alexander, C. M. D., Busemann, H., et al. 2010, *GeCoA*, **74**, 5966